J. Fluid Mech. (2013), *vol.* 730, *pp.* 593–606. © Cambridge University Press 2013
doi:10.1017/jfm.2013.351

Relationship between temporal and spatial averages in grid turbulence

L. Djenidi[1],†, S. F. Tardu[2] and R. A. Antonia[1]

[1]Discipline of Mechanical Engineering, School of Engineering, University of Newcastle, Newcastle, 2308 NSW, Australia

[2]Laboratoires des Ecoulements Geophysiques et Industriels, LEGI BP 53 X Grenoble, France

(Received 22 October 2012; revised 28 May 2013; accepted 8 July 2013;
first published online 2 August 2013)

A long-time direct numerical simulation (DNS) based on the lattice Boltzmann method is carried out for grid turbulence with the view to compare spatially averaged statistical properties in planes perpendicular to the mean flow with their temporal counterparts. The results show that the two averages become equal a short distance downstream of the grid. This equality indicates that the flow has become homogeneous in a plane perpendicular to the mean flow. This is an important result, since it confirms that hot-wire measurements are appropriate for testing theoretical results based on spatially averaged statistics. It is equally important in the context of DNS of grid turbulence, since it justifies the use of spatial averaging along a lateral direction and over several realizations for determining various statistical properties. Finally, the very good agreement between temporal and spatial averages validates the comparison between temporal (experiments) and spatial (DNS) statistical properties. The results are also interesting because, since the flow is stationary in time and spatially homogeneous along lateral directions, the equality between the two types of averaging provides strong support for the ergodic hypothesis in grid turbulence in planes perpendicular to the mean flow.

Key words: homogeneous, isotropic turbulence

1. Introduction

Since Taylor's (1935) pioneering work, it is common to experimentally investigate homogeneous and isotropic turbulence (HIT) by examining grid turbulence, generated by passing a uniform flow through a grid, usually made of vertical and horizontal bars, and placed normal to the main flow. It is generally accepted that grid-generated turbulence is the closest practical approximation to HIT, considered to be the simplest type of three-dimensional turbulence, which explains the considerable amount of work dedicated to this flow (see Ertunc *et al.* 2010, for a brief but recent review on grid turbulence).

The vast majority of grid turbulence measurements are performed using hot-wire (velocity measurements) and cold-wire (temperature measurements) anemometry. The information is temporal and obtained at fixed points relative to the grid. Taylor's

† Email address for correspondence: lyazid.djenidi@newcastle.edu.au

https://doi.org/10.1017/jfm.2013.351 Published online by Cambridge University Press

frozen turbulence assumption (Taylor 1938), which can be used to treat the change along the flow direction as a change in time (Batchelor 1953), is commonly employed to test theoretical spatial relations. The assumption, which plays a significant role in the study of grid-generated turbulence, is well satisfied when the turbulence intensity is small in comparison to the local mean velocity and the turbulence is homogeneous in space. In grid turbulence, which is considered axisymmetric with respect to x or the direction of the mean flow, the first condition is generally well satisfied, and the spatial decay along the main flow direction is assumed small over length scales comparable to the linear scale of the turbulence (Grant & Nisbet 1957) and thus neglected.

Only recently have direct numerical simulations (DNS) of grid turbulence with the grid itself within the computational domain become possible (e.g. Djenidi 2006; Ertunc *et al.* 2010; Djenidi & Tardu 2012). This permits carrying out meaningful comparisons between DNS and experiments, as well as exploring further grid turbulence and testing theoretical results more adequately. Direct comparisons between DNS results and hot-wire measurements can be carried out by comparing single-point temporal averages between the DNS and hot-wire data. But this would involve running the simulations over relatively long periods of time. To avoid this, one could perform spatial averaging on relatively few independent velocity fields. However, this supposes that spatial and temporal averages are equivalent, e.g. that the ergodic hypothesis, often used in turbulence, is valid. According to this hypothesis, if the turbulence is both statistically stationary in time and homogeneous in space, then its temporal and spatial statistical properties should be the same. Galanti & Tsinober (2004) performed a DNS of turbulence in a cubic domain with periodic conditions over a long time and showed that temporal and spatial statistical properties are equal. They argued that this equality supported the ergodic hypothesis. Although this hypothesis has been assumed in grid turbulence (Batchelor 1953, pp. 16, 17, see also Hinze 1975, p. 5), it has not yet been tested.

While grid turbulence is statistically stationary in time, it cannot satisfy ergodicity completely since it decays with increasing distance downstream of the grid. However, one may consider the ergodicity in planes perpendicular to the mean flow direction if the turbulence is spatially homogeneous in these planes. Grant & Nisbet (1957) studied the lateral inhomogeneity in turbulence from a grid made of horizontal and vertical bars in a biplane configuration. They reported the presence of lateral inhomogeneity in the turbulence intensity even at x/M as large as 80 (M is the mesh length). They suggested that for the inhomogeneity to be negligible, adjacent 'wakes' emanating from the bars should overlap appreciably. This seems to be supported by data from Ertunc *et al.* (2010) who used grids with different porosities. The recent DNS of Djenidi & Tardu (2012) of grid-generated turbulence, where the grid is made up of independent flat square elements with a solidity of $\sim$25 % (see figure 2 below) showed that while the lateral inhomogeneity was high in the region close to the grid ($x/M < 10$), it decreased significantly with increasing distance. However, the downstream extent was only $x/M = 15$, not long enough for the turbulence to reach a complete (lateral) homogeneous state. It was observed though that the grid configuration generates turbulence which tends to reach lateral homogeneity over a smaller distance than that for grids made of bars. This may be because the individual wakes generated by the square blocks interact more strongly and earlier than those generated by the vertical and horizontal bars. Corrsin (1963) proposed at least three criteria that must be satisfied for ensuring homogeneity in grid turbulence (grid made of horizontal and vertical bars): (i) large grid porosity; (ii) large L/M (L is the height/diameter of the wind tunnel); and (iii) measurements should be taken at

https://doi.org/10.1017/jfm.2013.351 Published online by Cambridge University Press

least $40M$ downstream of the grid. While these criteria can be easily satisfied in experiments, they may be problematic for DNS, in particular the last two, which may imply the use of a very large computational domain. We believe that for the grid made of square flat blocks with a solidity of 25 %, as used here, the last two criteria can be relaxed, thus allowing the use of a 'minimal' computational domain.

Ergodicity is the equality between ensemble averages and appropriately defined time or space averages obtained from a single sample. The necessary but not sufficient conditions for ergodicity are stationarity in time and homogeneity in space. The ergodic hypothesis, first introduced by Boltzmann (1884), essentially states that for every initial state, the time average of any measurable quantity converges to the average over space as time and space tend to infinity. This formulation is however not true in general (Nillsen 2010). Birkhoff (1931) has shown that if a process is ergodic, then time and space averages coincide and the Boltzmann ergodic hypothesis holds. The inverse is also true under measure-preserving transformations. The fine mathematical details are beyond the scope of this paper and we only briefly recall here a few ergodic theory elements (Cramer & Leadbetter 2004; Walter 1982). A transformation is measure-preserving when events occur with the same probability before and after transformation. The time (space) shift is measure-preserving (invariant) if the turbulence is stationary (homogeneous). Finally, if the quantity to measure is also ergodic, then time or space averages are equal to the ensemble averages. The latter element can be handled in a simpler way. The averages over samples ζ_i of a given quantity $\alpha(\boldsymbol{x}, t; \zeta_i)$ ($\boldsymbol{x} = (x, y, z)$ is a spatial position) depend in general on the sample ζ_i. The question is: under what conditions are space or time averages of α constant and independent of ζ_i? The answer is related to the specific statistics we deal with, such as mean and variances of the velocity field, probability distributions or correlation functions. The measure $\alpha(\boldsymbol{x}, t; \zeta_i)$ is mean ergodic in space if $\alpha(\boldsymbol{x} + \boldsymbol{r}, t; \zeta_i)$ and $\alpha(\boldsymbol{x}, t; \zeta_i)$ are uncorrelated for large $\boldsymbol{r}$ (Papoulis 1984). A more rigorous theoretical investigation conducted by Androulakis & Dostoglu (2004) who dealt directly with the Batchelor hypothesis leads to the same result.

Strictly speaking, testing ergodicity implies performing measurements over a very long time in one realization as well as over an infinite number of realizations. Such a procedure is obviously impractical. However, as mentioned earlier, if the system is statistically stationary in time and homogeneous in space then ergodicity implies that the temporal and spatial statistics are equal. Thus, the main purpose of the present work is to compare spatially averaged statistics in planes perpendicular to the mean flow with their temporal counterparts. Agreement between these two types of statistics could be interpreted, albeit indirectly, as providing support for the ergodic hypothesis. It is important to stress that determining whether a dynamics system, such as a turbulent flow, is ergodic or not is more than just an academic problem. In the case of turbulence for example, in order for the statistical theory to be useful as a method of describing the physics of turbulence, it is necessary to be able to measure quantities such as mean, variances and high-order moments of velocity fluctuations and relate them to the theoretical ones. It is therefore necessary that the temporal averages obtained from experimental samples be identified with corresponding (theoretical) ensemble averages. This is also true for spatial averages. These requirements can be fulfilled only when the ergodic hypothesis is satisfied. Thus, testing the ergodic hypothesis becomes critical for both experiments and DNS and its importance cannot therefore be overlooked.

https://doi.org/10.1017/jfm.2013.351 Published online by Cambridge University Press

2. Numerical procedure

2.1. *Lattice Boltzmann method*

The DNS is carried out using the lattice Boltzmann method (LBM). Rather than solving the governing fluid equations (Navier–Stokes equations), the LBM solves the Boltzmann equation on a lattice. The basic idea of the LBM is to construct a simplified kinetic model that incorporates the essential physics of microscopic average properties, which obey the desired (macroscopic) Navier–Stokes equations (Frisch, Hasslacher & Pomeau 1986). With a sufficient amount of symmetry of the lattice, the LBM implicitly solves these latter equations with second-order accuracy. For the present calculations, each computational node consists of a three-dimensional lattice composed of 18 moving particles and a rest particle (lattice model D3Q19; for a detailed account of LBM see Chen & Doolen 1998; Succi 2001). The spacings in the three directions between nodes are Δx, Δy and Δz.

The Boltzmann equation is discretized on the cubic lattice and results in the standard lattice Boltzmann equation (LBE) which, when combined with the Bhatnagar–Gross–Krook (BGK) approximation, governs the time and space variations of the single-particle distribution $f_i(\boldsymbol{x}, t)$ at the lattice site $\boldsymbol{x}$ and is expressed as:

$$f_i(\boldsymbol{x} + \boldsymbol{e}_i\Delta t, t + \Delta t) - f_i(\boldsymbol{x}, t) = -\frac{1}{\tau}(f_i(\boldsymbol{x}, t) - f_i^{eq}(\boldsymbol{x}, t)), \quad i = 0, 1, \ldots, 8, \tag{2.1}$$

where τ is the relaxation time, Δt the time step, $\boldsymbol{e}_i$ $(=\Delta\boldsymbol{x}/\Delta t)$ is the velocity of particle i in the i-direction and f_i^{eq} is the equilibrium single-particle distribution:

$$f_i^{eq} = \rho\omega_i(1 + 3(\boldsymbol{e}_i \cdot \boldsymbol{u}) + \tfrac{9}{2}(\boldsymbol{e}_i \cdot \boldsymbol{u})^2 - \tfrac{3}{2}u^2), \tag{2.2}$$

where $\rho(=\sum_i f_i)$ is the fluid density, $\boldsymbol{u}$ $(\rho\boldsymbol{u} = \sum_i f_i\boldsymbol{e}_i)$ is the local fluid velocity and ω_i is the corresponding weight ($\omega_i = 1/3$ for $i = 0$, $1/18$ for $i = 1$–6 and $1/36$ for $i = 7$–18; $i = 0$ corresponds to the rest particle at the centre of the lattice, $i = 1, \ldots, 6$ correspond to the particles on the axis aligned with x, y and z, and $i = 7, \ldots, 18$ are related to the particles on the diagonal directions). The relaxation time is related to the kinematic viscosity of the fluid via the relation

$$\nu = \frac{2\tau - 1}{6}. \tag{2.3}$$

In (2.1), $\Delta x = \Delta y = \Delta z = 1$ (x is the longitudinal direction and y and z the lateral directions). With this choice, $|\boldsymbol{e}_i| = 1$, for $i = 1$–6, and $\sqrt{2}$ for $i = 7$–18; note that $|\boldsymbol{e}_0| = 0$, and the variables such as $x, t, \boldsymbol{u}, \rho$ and ν are expressed in lattice units; ν is estimated once the Reynolds number is fixed ($\nu = U_0M/R_M$, see below for definitions).

The left-hand side of (2.1) is the so-called streaming operation, which means that the particles move to their nearest neighbours along the direction of their velocity (i.e. they radiate outwards from the centre of the cubic lattice). The right-hand side is the collision term, here modelled by the BGK collision operator, which describes the redistribution of the particles at each node (for more details on the LBM see, for example, Chen & Doolen 1998 or Succi (2001)). Thus, (2.1) is solved according to these two operations: collision and streaming. The collision step is described by

$$f_i^{new}(\boldsymbol{x}, t) = f_i(\boldsymbol{x}, t) - \frac{\Delta t}{\tau}(f_i(\boldsymbol{x}, t) - f_i^{eq}(\boldsymbol{x}, t)), \tag{2.4}$$

where f_i^{eq} is calculated using (2.2). The streaming process is described by

$$f_i(\boldsymbol{x} + \boldsymbol{e}_i\Delta t, t + \Delta t) = f_i^{new}(\boldsymbol{x}, t). \tag{2.5}$$

https://doi.org/10.1017/jfm.2013.351 Published online by Cambridge University Press

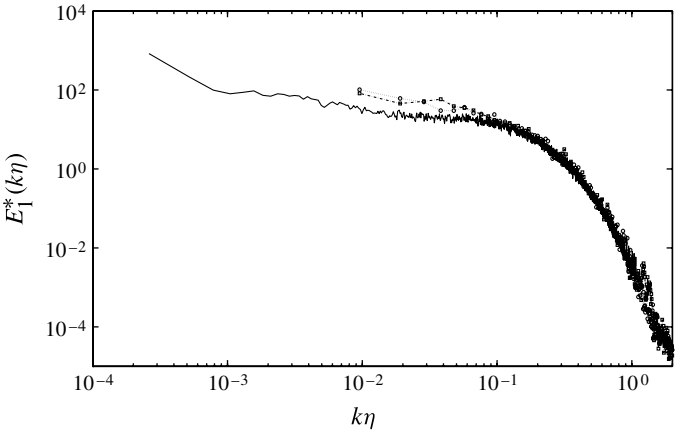


FIGURE 1. Kolmogorov normalized streamwise velocity spectra, $E_1^*(k\eta)$. Symbols: LBM at $x/M = 30$, *and*$z/D = 0$ (circles) and 1 (squares); solid line: measurements at $x/M = 460$.

The collisions are entirely local, making the LBM efficiently parallelized. At time t, the particle distributions are updated based on (2.4); then, at time $t + \Delta t$, the particles propagate according to (2.5).

In order to avoid the occurrence of instabilities where the magnitude of the local strain rate could be large, mainly around the grid, a large-eddy simulation (LES) scheme based on the Smagorinsky model and developed for LBM by Hou *et al.* (1996) was used. We briefly reproduce the scheme here. A turbulent viscosity is added to the kinematic viscosity as follows:

$$\nu_{total} = \nu + \nu_t \tag{2.6}$$

with

$$\nu_t = (C\Delta)^2|S| \tag{2.7}$$

where $C = 0.1$, $\Delta = \Delta x$. The term $|S|$, defined as

$$|S| = \frac{\sqrt{\nu^2 + 18(C\Delta)^2(\Pi_{ij}\Pi_{ij})^{1/2}} - \nu}{6(C\Delta)^2}, \tag{2.8}$$

is the intensity of the local filtered strain-rate tensor

$$\Pi_{\alpha\beta} = \frac{1}{2}\left(\frac{\partial u_\alpha}{\partial x_\beta} + \frac{\partial u_\beta}{\partial x_\alpha}\right) = \sum_i e_{i\alpha}e_{i\alpha}(f_i - f_i^{eq}). \tag{2.9}$$

The relation between the total viscosity and the relaxation time is now

$$\tau = 3\nu_{total} + \tfrac{1}{2}. \tag{2.10}$$

It can be seen that the value of τ is locally adjusted, depending in the value of $|S|$. Such adjustment occurs mainly in the near vicinity of the grid where relatively high velocity gradients may occur. To verify that the LES scheme does not induce spurious effects on the results, a spectral analysis was carried out and shown in figure 1, where two LBM spectra (computed from the time series) at $x/M = 30$ and two lateral positions ($z/D = 0$ and $z/D = 1$) are compared to a measured one in grid turbulence

https://doi.org/10.1017/jfm.2013.351 Published online by Cambridge University Press

at $x/M = 460$. The Taylor-microscale Reynolds number R_λ for both the simulation and experiment is about 20. The measurements were made using a single hot-wire probe and the grid is a mesh of interwoven wires with a diameter of 1 mm and a mesh size of ~5 mm. Clearly, the two numerical spectra collapse well with each other and with the experimental spectrum at sufficiently high wavenumbers; the difference at low wavenumbers reflects mainly the difference in grid geometry. The very good collapse between the LBM spectra and the measured spectrum indicates that the LES scheme does affect the results. This was expected because the LES filter size was set equal to the spatial resolution, which in turn is of the order of the Kolmogorov length scale (see below).

The motivation for the choice of the LBM over the classical resolution of the Navier–Stokes equations can be briefly summarized as follows: (i) extreme ease of solid surfaces implementation; (ii) no need for solving the Poisson equation for the pressure; and (iii), which follows in part from (ii), the collision step is local in nature, making the implementation of parallel computation extremely easy. The method has been successfully used for simulating turbulent flows (Burattini *et al.* 2006; Djenidi 2006, 2008; Ertunc *et al.* 2010; Djenidi & Tardu 2012).

2.2. *Computational domain and boundary conditions*

The computational uniform Cartesian mesh consists of $1600 \times 240 \times 240$ mesh points. The streamwise size of the computational domain is twice that of Djenidi & Tardu (2012). The turbulence-generating grid (placed at the x-node of 180) is made up of 6×6 floating flat square elements in an aligned arrangement (figure 2). Each element is represented by $1 \times 20 \times 20$ mesh points and the mesh spacing (M) between the centre of two elements is 40 mesh points (i.e. $2D$), yielding a grid solidity of 0.25. The downstream distance extends to $x/D = 70$ (equivalently $x/M = 35$), where the origin of x is the grid plane and $D = 20$ mesh points is the block side length. Note that the same distance would require far too large a number of mesh points if a grid made of vertical and horizontal bars and with the same solidity were to be used. This is the main reason why the square elements were chosen. Periodic conditions are applied in the y- and z-directions. At the inlet, a uniform velocity ($U_0 = 0.05$, and $V_0 = W_0 = 0$) is imposed, and a convective boundary condition is applied at the outlet. It was observed that the convective condition affected marginally the simulation results within a distance of less than $1D$ upstream of the outlet. A zero-gradient boundary condition was also tried at the outlet and no significant difference was observed. Although these are relatively simple boundary conditions, they are quite suitable for the present simulation for at least three reasons: (i) absence of solid walls at the outlet; (ii) slow change in the velocity field within the outlet region; and (iii) the relatively fine computational mesh resolution, which is what is commonly encountered in DNS. Implementing other more sophisticated outlet boundary conditions such as that proposed by Chikatamarla, Ansumali & Karlin (2006) or investigated by Carver *et al.* (2012) would not change the results and might increase the computational time. The no-slip condition at the grid elements is enforced through a bounce-back scheme (Succi 2001). The Reynolds number based on mesh spacing, R_M, is about 3200. This is a relatively small value, which allows a reasonably good computational mesh resolution which varies from $\sim 2.9\eta$ at $x/D = 8$ to 0.78η at $x/D = 68$; η is the Kolmogorov length scale. The (statistically) steady-state solution is obtained after 30 000 time steps. The first velocity field is saved after 10^5 time steps. Subsequently, 100 velocity fields are recorded, each separated by about 10 000 time

https://doi.org/10.1017/jfm.2013.351 Published online by Cambridge University Press

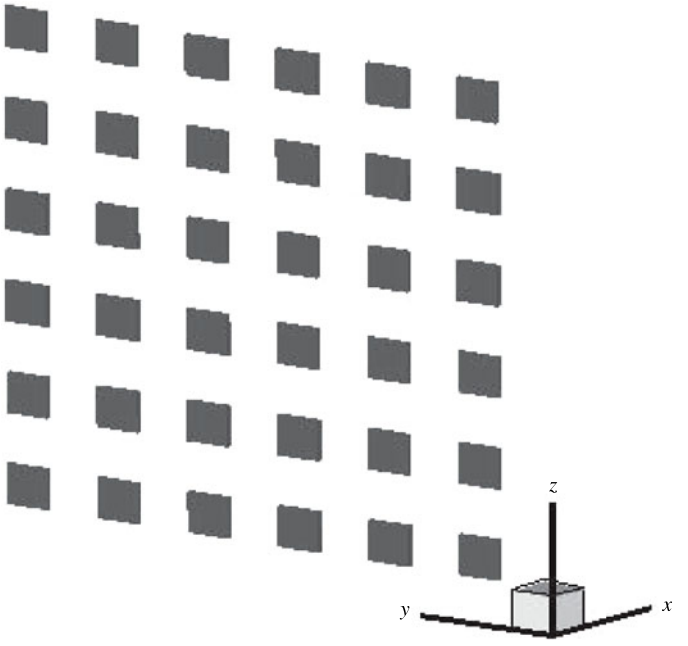


FIGURE 2. Floating square elements forming the grid. Note that for clarity, the reference axes have been shifted from the position ($x = y = z = 0$), which is at the geometrical centre of the grid. The flow is in the positive direction of the x-axis.

steps (about $8.5\lambda/u'$, u' is the root-mean-square velocity fluctuation at $x/D = 50$) to ensure that consecutive fields are uncorrelated.

The Taylor microscale Reynolds number, R_λ, varies from $\sim$60 at $x/D = 8$ to $\sim$18 at $x/D = 70$. It should be noted that, immediately downstream of the grid, R_λ increases rapidly to a maximum of about 1300 at $x/D = 0.5$ then, as turbulence begins to decay, decreases quickly to reach 92 at $x/D = 5$; beyond this position, the rate at which R_λ decreases is reduced. For example, $R_\lambda = 25$ at $x/D = 30$ and $R_\lambda = 19$ at $x/D = 65$. The strong drop in R_λ indicates a transient stage. Beyond that regime, R_λ is comparable to the values of Batchelor & Townsend (1947) ($R_\lambda \simeq 20$ for $20 \leqslant x/M \leqslant 120$) where $R_M = 5620$.

3. Results

3.1. *Spatial homogeneity*

Before comparing the single-point temporal averages with the spatial averages in planes perpendicular to the mean flow, one must first verify the spatial homogeneity in those planes. For this purpose, long time series (about 773 times λ/u') are recorded at various downstream positions behind the grid. The first set of signals is taken along the grid centreline between four adjacent blocks. The second is taken along a line perpendicular to the centre of a block.

Figure 3 shows the probability density function $p(v)$ (p.d.f.) of the transverse velocity component, v, defined as:

$$p(v) = \text{p.d.f.}\left(\frac{v - \overline{v}}{\sigma_v}\right), \tag{3.1}$$

https://doi.org/10.1017/jfm.2013.351 Published online by Cambridge University Press

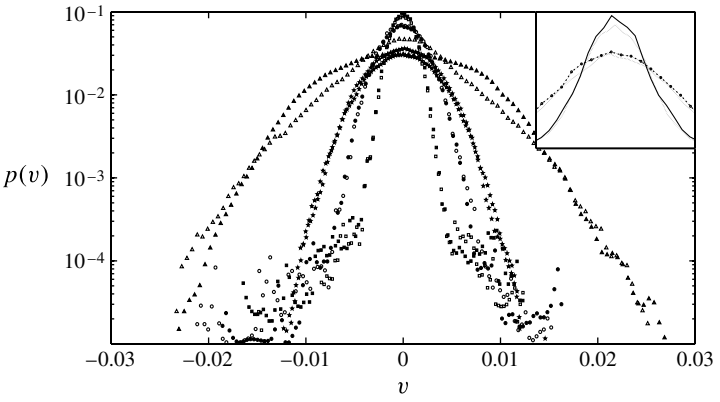


FIGURE 3. p.d.f. $p(v)$ at $x/D = 8.5$ (triangles), 18.5 (stars), 28.5 (circles) and 53.5 (squares), and $y = z = 0$ (open symbols) and $y = z = D$ (filled symbols). Inset: enlarged region $-0.003 \leqslant v \leqslant 0.003$. Only locations $x/D = 28.5$ and 53.5 are represented.

where the overbar denotes the time average and σ_v the standard deviation of v. For convenience, we will denote

$$\overline{v} = \langle v(\boldsymbol{x}) \rangle_T = \frac{1}{T} \int_{t_0}^{t_0+T} v(\boldsymbol{x}, t)\, \mathrm{d}t \tag{3.2}$$

where $\boldsymbol{x} = (x, y, z)$ is a fixed spatial position. Notice first the occurrence of relatively large values of v ($\sim$40 % of the mean velocity U at $x/D = 28.5$ and 30 % at $x/D = 53.5$) in the tails of the p.d.f.s, which suggests that computing the ensemble average for directly testing ergodicity requires a very large number of realizations. Close to the grid ($x/D = 8.5$), the distributions change with the lateral position, highlighting the non-homogeneity of the flow in the near-grid region. For example, notice the flatter shape of the distribution at $y = z = D$ for $-0.01 \leqslant v \leqslant 0.01$. As x/D increases, the difference in $p(v)$ between the two lateral locations reduces considerably. At $x/D = 18.5$, the distributions at the two lateral positions are close to each other, whereas they are nearly indistinguishable for $x/D \geqslant 28.5$. These results indicate that the turbulence becomes spatially homogeneous in the lateral directions at $x/D \sim 20$. This is reinforced in figures 4 ($x/D = 8.5$) and 5 ($x/D = 28.5$) showing the bivariate histogram between u and v, which for convenience is referred to as pseudo-joint p.d.f. and denoted $psp(u, v)$; the relation between $psp(u, v)$ and the joint p.d.f., $p(u, v)$, is $p(u, v) = psp(u, v)/N_{bin}$, where N_{bin} is the number bin elements used to compute $psp(u, v)$. At the first x position, $psp(u, v)$ at $y = z = 0$ differs markedly from its counterpart at $y = z = D$ (figure 4), contrasting strongly with the distributions at $x/D = 28.5$ which are similar and almost perfectly circular (figure 5). This is further illustrated in figure 6, which shows the difference in $psp(u, v)$, at the two lateral locations. Notice the strong reduction in the difference when x/D varies from 8.5 to 28.5. Also of interest is the significant difference between the two plots in figure 6, namely at $x/D = 8.5$ (figure 6*a*), the maximum difference is located away from the centre (0.0), while at $x/D = 28.5$ (figure 6*b*) it is at centre. The lateral homogeneity is further illustrated in figure 7 showing the mean velocity components U and V, the variance of the transverse velocity component w, the Taylor microscale, λ $(=(\langle u^2 \rangle \langle (\partial u/\partial x)^2 \rangle)^{1/2})$, and the variance of the second-order velocity

https://doi.org/10.1017/jfm.2013.351 Published online by Cambridge University Press

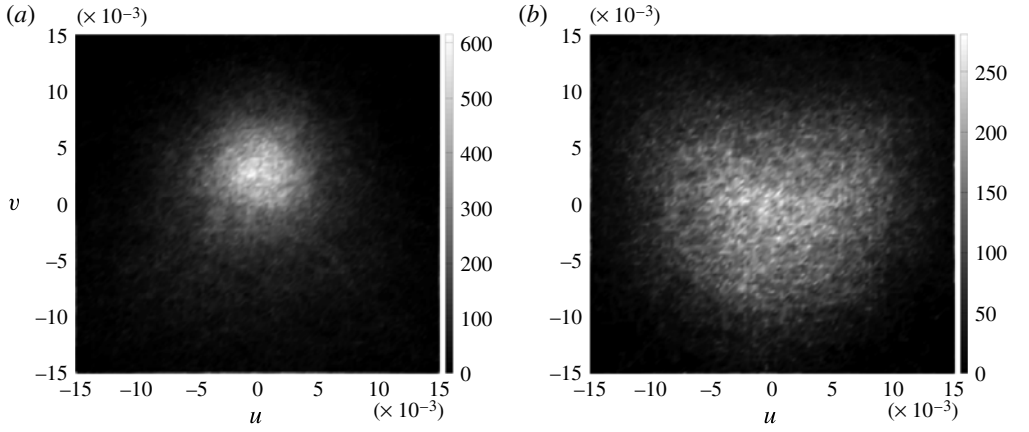


FIGURE 4. Pseudo-joint p.d.f.s of u and v at $x/D = 8.5$ and (*a*) $y = z = 0$ and (*b*) $y = z = D$. The colourmaps are used only as a guide.

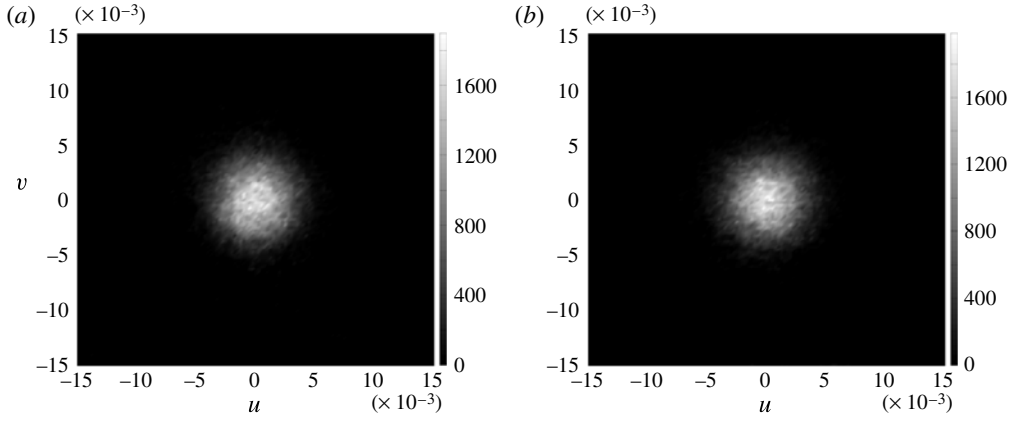


FIGURE 5. Pseudo-joint p.d.f.s of u and v at $x/D = 28.5$ and (*a*) $y = z = 0$ and (*b*) $y = z = D$. The colourmaps are used only as a guide.

derivative, $\partial^2 u/\partial x^2$ (the temporal derivative was converted into a spatial derivative via Taylor's hypothesis $x = U_c t$, where the convective velocity U_c is taken equal to U_0). Notice that there is virtually no difference between the two lateral positions for $x/D \geqslant 15$. The lateral velocity component $\langle V \rangle$ is zero immediately behind the grid at the two lateral locations, as expected by symmetry.

3.2. *Temporal and spatial statistics*

The previous section indicates that the turbulence downstream of the grid can be considered spatially homogeneous in planes perpendicular to the mean flow for $x/D \geqslant 20$. Since the turbulence is also statistically stationary, we will next test the two types of averages. As stated earlier, if the ergodic hypothesis in planes perpendicular to the mean flow is satisfied then $\langle Q(x) \rangle_T = \langle Q(x,t) \rangle_S$ where $\langle Q(x,t) \rangle_S$ is a spatial

https://doi.org/10.1017/jfm.2013.351 Published online by Cambridge University Press

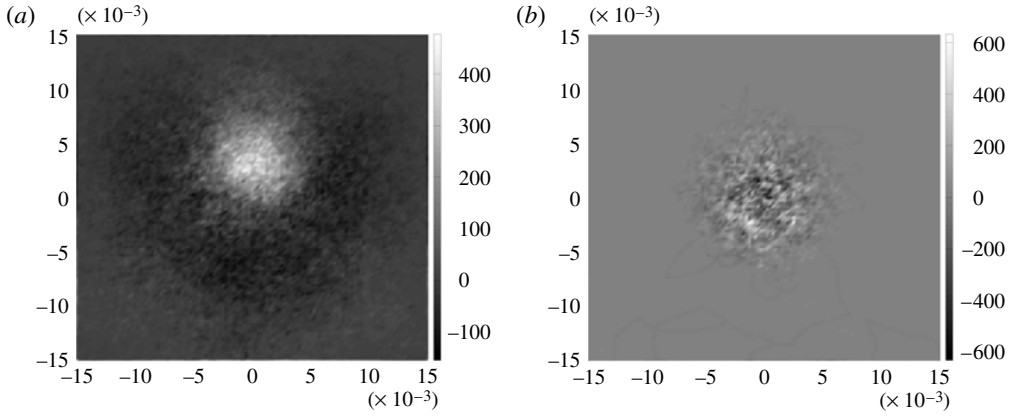


FIGURE 6. Difference in the pseudo-joint p.d.f.s of u and v at $y = z = 0$ and $y = z = D$ for (a) $x/D = 8.5$ and (b) $x/D = 28.5$. The colourmaps are used only as a guide.

average in planes perpendicular to the mean flow and defined as:

$$\langle Q(x,t)\rangle_S = \frac{1}{S}\iint_S Q(\boldsymbol{x},t)\,\mathrm{d}y\,\mathrm{d}z \tag{3.3}$$

with S representing the entire transverse plane (y, z) (see figure 2). In (3.3), the spatial integration is carried out over one randomly selected realization (one velocity field). Figure 7 compares $\langle Q(x)\rangle_T$ with $\langle Q(x,t)\rangle_S$. The figure also shows the lateral spatial averaging over 66 realizations. The good correspondence between 1 and 66 realizations points to the ergodic nature of the quantities investigated, despite the inevitable noise associated with the single realization (due to the finite domain, which limits the lateral extent of the spatial averaging). Clearly, the square root of the 'noise' between one realization and converged statistics goes to zero as the size of the sample is increased. That is precisely the definition of mean-ergodic processes. Whether or not all possible measures needed to describe the turbulence behind a grid are ergodic is of course an entirely open question.

There is a perfect match in figure 7 between the spatial averages ($\langle\cdot\rangle_S$) of the various quantities and their temporal counterparts ($\langle\cdot\rangle_T$), demonstrating the equivalence between the two types of averaging. It is not quite clear why the correspondence between the spatial averaging for one realization and temporal averaging is better for velocity derivatives than velocity fluctuations. Galanti & Tsinober (2004), who reported similar differences, speculate that the better agreement between the temporal and (one-realization) spatial statistics associated with the field of velocity derivatives is the phenomenon of self-amplification of the velocity field in three-dimensional turbulence, which is not affected by the large-scale motion.

Further illustration of the equivalence between the two averages is seen in the good agreement between the temporal and spatial p.d.f.s of v (figure 8; the same is observed for the other velocity components). The differences seen at large values of v are due to an insufficient separation between the integral length scale and the size of the computational domain. This is more pronounced at $x/D = 53.5$ than at $x/D = 28.5$; the integral length scale is larger at the latter station, while the dimensions of the lateral sides are kept constant. Galanti & Tsinober (2004) observed a similar feature in their three-dimensional box turbulence simulation.

https://doi.org/10.1017/jfm.2013.351 Published online by Cambridge University Press

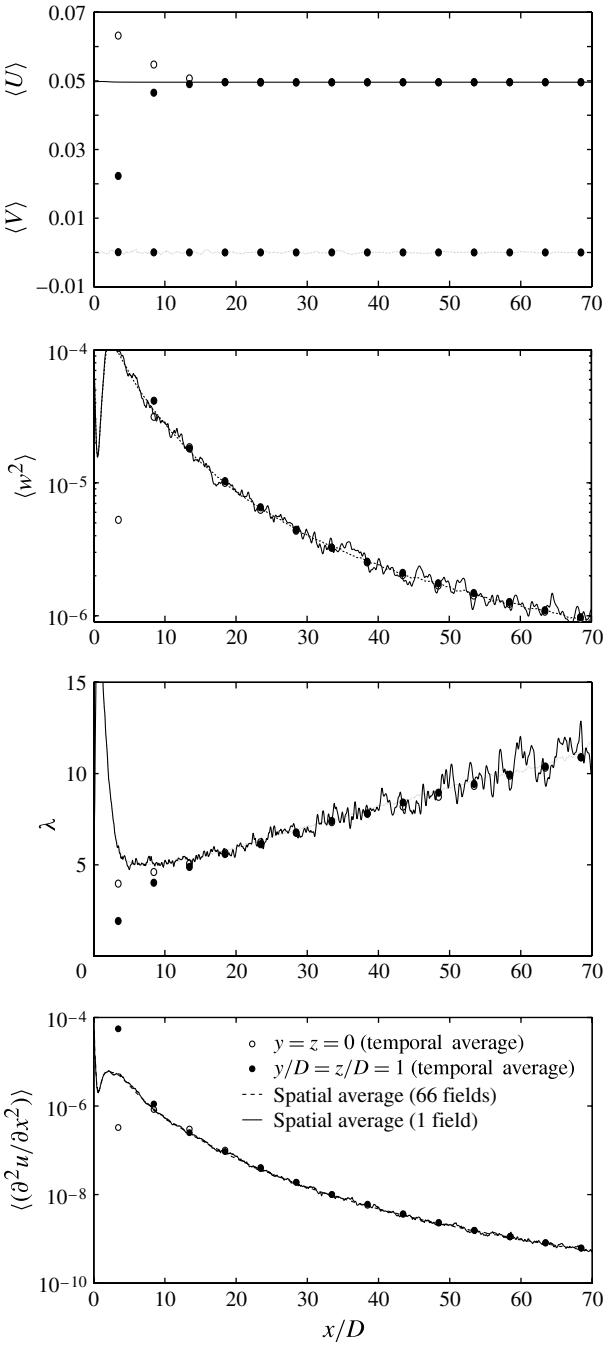


FIGURE 7. Streamwise variations of temporal (symbols) and spatial (lines) averages of $\langle U \rangle$, $\langle V \rangle$, $\langle w^2 \rangle$, λ and $\langle (\partial^2 u/\partial x^2) \rangle$. The temporal averages are calculated at two lateral locations. A linear-log scale is used for $\langle w^2 \rangle$ and $\langle (\partial^2 u/\partial x^2) \rangle$. Note that because the 66 fields and 1 field averages for both U and V collapse, we only plot the 66-fields average for U and 1-field average for V. Note also that the open circles for the temporal average of V are hidden by the filled ones.

https://doi.org/10.1017/jfm.2013.351 Published online by Cambridge University Press

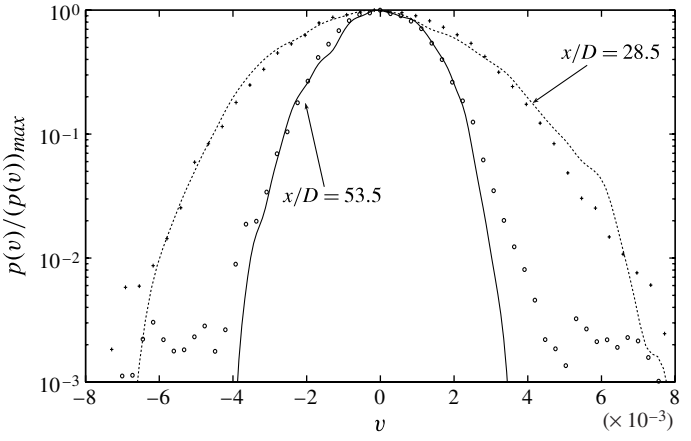


FIGURE 8. P.d.f. $p(v)$ at $x/D = 28.5$ and 53.5, and $y = z = 0$. Temporal p.d.f.: symbols; spatial p.d.f.: lines.

Batchelor (1953) pointed out that it is the objective of the ergodic theory to show that the spatial average is the same for all realizations and is identical to the ensemble average, and simply assumed this to be the case for grid turbulence. Androulakis & Dostoglu (2004) provided rigorous proofs that in homogeneous flow not only does the spatial average almost always exist, but that it is equal to the ensemble average, if ergodicity is valid. The brief ergodic theory outlined in the introduction and the data of figures 7 and 8 suggest that the spatial average in a plane perpendicular to the mean flow is equal to the ensemble average, and provide strong support for the ergodic hypothesis, at least for the variables presented.

4. Concluding remarks

A long-time DNS of grid turbulence, implemented with the lattice Boltzmann method, shows that the turbulence becomes homogeneous in planes perpendicular to the mean flow at a relatively short distance downstream of the grid. For the present geometry, with a grid made of flat square blocks and a solidity of 25 %, this distance is about $20D$ (or $\sim 10M$). The results also indicate that temporal and (lateral) spatial statistical properties are equal, lending strong support to the validity of ergodicity in grid turbulence in planes perpendicular to the mean flow. This is a significant result. In the majority of turbulence research, it is generally thought self-evident that temporal and spatial averages are equivalent. This equivalence is often assumed without being tested. The present work, which shows for the first time that ergodicity is well satisfied in grid turbulence in planes perpendicular to the mean flow, demonstrates unequivocally the equivalence between temporal and spatial averages when homogeneity is valid. It definitely confirms that hot-wire measurements are appropriate for testing theoretical results based on spatially averaged statistics. It is equally important for DNS of grid turbulence, since it justifies carrying out spatial lateral averaging using several realizations, to determine various statistical properties. Finally, the very good agreement between the temporal and spatial averages validates the comparison between the temporal (experiments) and spatial (DNS) statistical properties. It should be recalled that the spatial resolution of the hot wire must be adequate. For example, the sensitive length of the hot wire should not exceed 3η to

https://doi.org/10.1017/jfm.2013.351 Published online by Cambridge University Press

minimize the errors associated with spatial integration of the wires (for a detailed discussion on the effects of wire length on the measurements see for example Ashok *et al.* 2012).

An analogy can be drawn with the DNS of turbulent channel flow, where temporal and spatial statistics in planes parallel to the wall are assumed equal. Since comparisons between DNS and experiments support this assumption, ergodicity, without ever being tested or verified, is validated implicitly because the flow is stationary in time and spatially homogeneous in (x, z) planes (z is the transverse direction) at fixed positions from the wall. Based on the present results, one may conjecture that the ergodic hypothesis can be valid in a turbulent channel flow at fixed positions from the wall. An obvious extension of this conjecture is that ergodicity in a turbulent boundary layer along a line perpendicular to the mean flow and parallel to the wall (i.e. at fixed points from the wall in the transverse direction) can also be valid. Galanti & Tsinober (2004) speculate that the ergodic hypothesis in non-homogeneous flows can be expected to be valid along coordinates for which homogeneity applies, or that one can at least expect that temporal and spatial statistical properties to be equal. Clearly, the present study, which follows and extends that of Galanti and Tsinober, supports their speculation. Interestingly, the validity of the ergodic hypothesis unambiguously allows linking of measurements (as represented here by the single-point time series) to the Navier–Stokes equations.

Finally, the results indicate that systematic checks on the homogeneity of the flow must be carried out before undertaking any statistical analysis for which homogeneity is required. For example, in the case of grid turbulence, it is important to determine the distance downstream of the grid where the flow becomes approximately homogeneous. Failing to perform such checks may lead, for instance, to an incorrect estimate of the power-law decay n for q ($q \sim x^n$, where q is twice the turbulent kinetic energy) or inadequate tests for local isotropy since one may inadvertently include data within a non-homogeneous region where ergodicity is not valid.

Acknowledgements

The financial support of the Australian Research Council is greatly acknowledged. L.D. wishes to thank the University of Joseph Fourier (Grenoble) for its financial support. L.D. and R.A.A. also thank Mr M. D. Kamruzzaman for providing the experimental data.

REFERENCES

ANDROULAKIS, G. & DOSTOGLU, S. 2004 Space averages and homogeneous fluid flows. *Math. Phys. Electron. J.* **10**, 1–12.

ASHOK, A., HULTMARK, M., BAILEY, S. C. C. & SMITS, A. J. 2012 Hot wire spatial resolution effects in measurements of grid generated turbulence. *Exp. Fluids* **53**, 1713–1722.

BATCHELOR, G. K. 1953 *The Theory of Homogeneous Turbulence*. Cambridge University Press.

BATCHELOR, G. K & TOWNSEND, A. A. 1947 Decay of vorticity in isotropic turbulence. *Proc. R. Soc. Lond.* A **190**, 534–550.

BIRKHOFF, G. D. 1931 Proof of the ergodic problem. *Proc. Natl Acad. Sci. USA* **17**, 600–656.

BOLTZMANN, L. 1884 Uber die Eigenschaften Monozyklischer und Amderer damit ver vandter Systeme. *Crelle's J.* **98**, 68–94.

BURATTINI, P., LAVOIE, P., AGRAWAL, A., DJENIDI, L. & ANTONIA, R. A. 2006 On the power law of decaying homogeneous isotropic turbulence at low R_λ. *Phys. Rev.* E **73**, 066304.

https://doi.org/10.1017/jfm.2013.351 Published online by Cambridge University Press

CARVER, H. B., NASH, R. W., BERNABEU, M. O., HETHERINGTON, J., GROEN, D., KRGER, T. & COVENEY, P. V. 2012 Choice of boundary condition and collision operator for lattice-Boltzmann simulation of moderate Reynolds number flow in complex domains. *Phys. Rev.* E (arXiv preprint, arXiv:1211.0205).

CHEN, S. & DOOLEN, G. D. 1998 Lattice Boltzmann method for fluid flows. *Annu. Rev. Fluid Mech.* **30**, 329–364.

CHIKATAMARLA, S. S., ANSUMALI, S. & KARLIN, I. V. 2006 Grad's approximation for missing data in lattice Boltzmann simulations. *Europhys. Lett.* **74**, 215–221.

CORRSIN, S. 1963 *Turbulence: Experimental Methods*, vol. 8. Springer.

CRAMER, H. & LEADBETTER, M. R. 2004 Stationary and related stochastic processes. In *Sample Function Properties and their Applications*. Dover.

DJENIDI, L. 2006 Lattice Boltzmann simulation of grid-generated turbulence. *J. Fluid Mech.* **552**, 13–35.

DJENIDI, L. 2008 Study of the structure of a turbulent crossbar near-wake by means of Lattice Boltzmann. *Phys. Rev.* E **77**, 036310.

DJENIDI, L. & TARDU, S. F. 2012 On the anisotropy of a low-Reynolds-number grid generated turbulence. *J. Fluid Mech.* **702**, 332–353.

ERTUNC, L., OZYILMAZ, N., LIENHART, H., DURST, F. & BERONOV, K. 2010 Homogeneity of turbulence generated by static-grid structures. *J. Fluid Mech.* **654**, 473–500.

FRISCH, U., HASSLACHER, B. & POMEAU, Y. 1986 Lattice gas automata for the Navier–Stokes equations. *Phys. Rev. Lett.* **56**, 1505–1508.

GALANTI, B. & TSINOBER, A. 2004 Is turbulence ergodic? *Phys. Lett.* **A**, 173–180.

GRANT, H. L. & NISBET, I. C. T. 1957 The inhomogeneity of grid turbulence. *J. Fluid Mech.* **2**, 263–272.

HINZE, J. O. 1975 *Turbulence*. McGraw-Hill Classic Textbook Reissues Series.

HOU, S., STERLIN, J., CHEN, S. & DOOLEN, G. D. 1996 A lattice Boltzmann subgrid model for high Reynolds number flows. In *Field Institute Communications. Pattern Fornmation and Lattice Gas Automata* (ed. A. T. Lawniczak & R. Kapral), vol. 6, pp. 151–166. American Mathematical Society. Also arXiv:comp-gas/9401004v1.

MONIN, A. S. & YAGLOM, A. M. 1971 *Statistical Fluid Mechanics*, vol. 1. MIT.

NILLSEN, R. 2010 *Randomness and Recurrence in Dynamical Systems*. The Carus Mathematical Monographs, vol. 31. Mathematical Association of America.

PAPOULIS, A. 1984 *Probability, Random Variables, and Stochastic Processes*, 2nd edn. McGraw Hill.

SUCCI, S. 2001 The lattice Boltzmann equation for fluid dynamics and beyond. In *Numerical Mathematics and Scientific Computation* (ed. G. H. Golub, R. Jeltsch, W. A. Light & E. Süli). Oxford University Press.

TAYLOR, G. I. 1935 Statistical theory of turbulence. *Proc. R. Soc. Lond.* A **151**, 412–478.

TAYLOR, G. I. 1938 The spectrum of turbulence. *Proc. R. Soc. Lond.* A **164**, 476–490.

WALTER, P. 1982 An Introduction to Ergodic Theory. Graduate Texts in Mathematics, vol. 79. Springer.

https://doi.org/10.1017/jfm.2013.351 Published online by Cambridge University Press